Experimental T33-stress Formulation of Test Specimen Thickness Effect on Fracture Toughness in the Transition Temperature Region

T. Meshii, et. al., Engineering Fracture Mechanics, **77**, 867-877 (2010).

Experimental T_{33}-stress Formulation of Test Specimen Thickness Effect on Fracture Toughness in the Transition Temperature Region

Toshiyuki MESHII [a]*, Tomohiro TANAKA [b]

[a] Graduate School of Engineering, University of Fukui, 3-9-1 Bunkyo, Fukui, Fukui, JAPAN.

[b] Graduate Student, University of Fukui, 3-9-1 Bunkyo, Fukui, Fukui, JAPAN.

*Correspondent, E-mail: meshii@u-fukui.ac.jp, FAX : +81-776-27-9764

Abstract

This paper describes a study of the test specimen thickness effect on fracture toughness of a material, in the transition temperature region, for CT specimens. In addition we studied the specimen thickness effect on the T_{33}-stress (the out-of-plane non-singular term in the series of elastic crack-tip stress fields), expecting that T_{33}-stress affected the crack-tip triaxiality and thus constraint in the out-of-plane direction. Finally, an experimental expression for the thickness effect on the fracture toughness using T_{33}-stress is proposed for 0.55% carbon steel S55C. In addition to the fact that T_{33} (which was negative) seemed to show an upper bound for large *B/W*, these results indicate the possibility of improving the existing methods for correlating fracture toughness obtained by test specimen with the toughness of actual cracks found in the structure, using T_{33}–stress.

Key words: Fracture mechanics; Elastic T-stress, Constraint effect, Fracture toughness, Cleavage, Transition temperature, CT-specimen, Thickness effect.

1. Introduction

The limited ability of a single parameter such as the stress intensity factor (SIF) K or J-Integral J to fully characterize crack tip conditions irrespective of geometry and load level has been recognized for years [1, 2]. To overcome this problem, two parameter descriptions of the crack-tip stress-strain state have been studied over the past three decades. The so-called elastic T-stress, or the second term of the Williams [3] series expansion for linear elastic crack tip fields, has been one of the strong candidate as the second parameter in this two-parameter approach. Larsson and Carlsson [2], and Rice [4] showed that the sign and magnitude of the T-stress substantially changes the size and shape of the plane strain crack tip plastic zone at finite load levels. Bilby et al. [5] showed that the T-stress can strongly affect the magnitude of hydrostatic triaxiality in the near crack tip elastic–plastic fields. The important result emerging from these referenced works is that the sign and magnitude of the T-stress can substantially alter the level of crack tip stress triaxiality and hence influence crack tip constraint. A positive T-stress strengthens the level of crack tip stress triaxiality and leads to high crack tip constraint, while a negative T-stress reduces the level of crack tip stress triaxiality and leads to the loss of the crack tip constraint. Though the T-stress is an elastic parameter, the later works by Al-Ani and Hancock [6], Betegon and Hancock [7], Du and Hancock [8] and O'Dowd and Shih [9] indicate that the T-stress, in addition to the J, provides a practical two-parameter characterization of plane strain elastic–plastic crack tip fields (corresponding to, for example, materials in the lower to mid-transition temperature range and referred to as "cleavage after significant plastic deformation, but before the initiation of ductile growth" by some researchers [10]) for a variety of crack configurations and loading conditions. These studies were focused on 2D (in-plane) crack tip constraint issues, and thus, the methodology was effective for issues such as explaining the effect of crack depth on the fracture toughness testing [10]. Hereafter, in-plane *T*-stress will be denoted as T_{11} (Fig. 1).

On the other hand, out-of-plane crack tip constraint as in the test specimen thickness (hereafter, TST) effect, which is also known to have a significant influence on the facture behavior of materials [11], cannot be expressed by the in-plane constraint parameter T_{11}. This is because the out-of-plane T_{33} and T_{11} are independent for general 3D cracks [12]. Instead, a practical expression, such as K_{Jc} ($\propto J_c^{\ 1/2}$) $\propto B^{-1/4}$ (K_{Jc}, J_c: fracture toughness of a material in the lower to mid-transition temperature range, B: TST) was proposed based on the weakest link model [11]. Considering the fact that it is not easy to correlate the fracture toughness obtained from a test specimen with that of a crack found in structures, it seemed appropriate that the TST effect on the fracture toughness be formulated with some crack tip constraint parameter, such as T_{33}.

Thus in this paper, the TST effect on the fracture toughness of a material in the transition temperature region was considered for CT specimens. Then, the TST effect on the T_{33} was studied, expecting that T_{33}-stress affected the crack-tip triaxiality and thus constraint in the out-of-plane direction. Finally, an experimental expression for the TST effect on the fracture toughness by using T_{33} is proposed for 0.55%

carbon steel S55C, tested by CT specimen.

2. Experimental T_{33}–Stress Formulation of TST Effect on Fracture Toughness

2.1. T-stresses

In an isotropic linear elastic body containing a crack subjected to symmetric (mode I) loading, the leading terms (up to order *O*(1)) in a series expansion of the stress field very near the crack front are [13]

$$\begin{Bmatrix} \sigma_{11} \\ \sigma_{22} \\ \sigma_{33} \\ \tau_{12} \\ \tau_{23} \\ \tau_{31} \end{Bmatrix} = \frac{K_I}{\sqrt{2\pi r}} \begin{Bmatrix} \cos\frac{\theta}{2}\left(1-\sin\frac{\theta}{2}\sin\frac{3\theta}{2}\right) \\ \cos\frac{\theta}{2}\left(1+\sin\frac{\theta}{2}\sin\frac{3\theta}{2}\right) \\ 2\nu\cos\frac{\theta}{2} \\ \sin\frac{\theta}{2}\cos\frac{\theta}{2}\cos\frac{3\theta}{2} \\ 0 \\ 0 \end{Bmatrix} + \begin{Bmatrix} T_{11} \\ 0 \\ T_{33} \\ 0 \\ 0 \\ 0 \end{Bmatrix} \tag{1}$$

$$T_{33} = E\varepsilon_{33} + \nu T_{11} \tag{2}$$

where r and θ are the in-plane polar coordinates of the plane normal to the crack front as shown in Fig. 1 and K_I is the local mode I stress intensity factor at location A. Here x_1 is the direction formed by the intersection of the plane normal to the crack front and the plane tangential to the crack plane. The terms T_{11} and T_{33} are the amplitudes of the second order terms in the three-dimensional series expansion of the crack front stress field in the x_1 and x_3 directions, respectively.

2.2. Research Plan

In this work we focused on the elastic parameter T_{33} (the out-of-plane non-singular term in the series of elastic crack-tip stress fields), expecting that T_{33}-stress affected the crack-tip triaxiality and thus constraint in the out-of-plane direction. Fracture toughness tests on CT test specimens, which had the same in-plane geometry but different thickness, were conducted to determine how the TST affected fracture toughness. Besides these tests, 3D elastic finite element analysis (FEA) was conducted for the different test specimens under identical nominal 2D SIF. In this case, it was expected that the in-plane elastic parameters K and T_{11} evaluated from the 3D FEA results would have close to the same values at the wall thickness center and the out-of plane parameter T_{33} would be dependent on thickness B. If significant changes were observed, an attempt would be made to formulate the TST effect on toughness with T_{33}. Finally, elastic-plastic FEA corresponding to the test results were run for comparison.

2.3. Fracture toughness tests

2.3.1. Material

The tested material was 0.55% carbon steel (JIS S55C), which is known to be in the transition temperature region at room temperature. The specimens were quenched at 850 ^{o}C and tempered at 650 ^{o}C. Chemical contents and tensile properties of the heat treated specimens are summarized in Tables 1 and 2, respectively. Tensile test was conducted in accordance with JIS Z2241 [14]. Test specimen configuration is given as Fig. 2. Two tests were conducted. The loading rate of the tensile test was 10 MPa/sec below the 0.2% strain and 40 % /min (measured at the gage length) for over 0.2%, which satisfied the JIS Z2241 [14] requirements of 3～30 MPa/sec below the 0.2% strain and 20~50% /min (measured at the gage length) for over 0.2%. Tensile test temperature was 20 ^{o}C.

2.3.2. Test specimens

Test specimen configuration was designed basically in accordance with the ASTM E399 [15], as shown in Fig. 3. The width W was set at 25 mm for all specimens. In addition to the standard ASTM thickness to width ratio B/W = 0.5, specimens with B/W = 0.25 and 0.4 (with side grooves; net thickness B_N = 0.8 B) were prepared. The crack length a after inserting fatigue crack satisfied ASTM's requirement of a/W = 0.45~0.55. Fatigue precrack was inserted at 20 ^{o}C under loads sufficiently below fracture toughness as shown in Table 3. Fatigue crack growth was monitored by clip gage. Five tests were conducted for each test specimen geometry.

2.3.3. Test results

The fracture toughness test was conducted in accordance with ASTM E399 [15]. Fracture toughness tests results are summarized in Table 4. Temperature for fracture toughness test was 20 ^{o}C. Here, the K_{max} in the table was obtained as the SIF K corresponding to the maximum load P_{max} from the following equation in ASTM E399 [15]:

$$K = \frac{P}{\sqrt{BB_N W}} f\left(\frac{a}{W}\right) \quad (3)$$

Figure 4 shows a typical load versus load-line crack opening displacement curve. As seen in this figure, P_{max} and P_{Q} (defined in ASTM E399) did not satisfy the condition $P_{\mathrm{max}}/ P_{\mathrm{Q}} < 1.1$, thus the fracture toughness expressed in the terms of SIF K_{Q} could not be interpreted as the plane strain fracture toughness. Therefore, we evaluated the fracture toughness in terms of J-integral, and named it $J_{\mathrm{c\,max}}$, in accordance with the method outlined in ASTM E1820 [16].

Next, a log-log plot of the relationship between the fracture toughness $J_{c\,max}$ and B/W is shown in Fig. 5. Note that this $J_{c\,max}$ reflected the actual measured crack length given in Table 4. From Fig. 5, the fracture toughness $J_{c\,max}$ is seen to be proportional to $(B/W)^{(-1/2)}$, and thus also proportional to $B^{(-1/2)}$ for our tests, though the scatter in $J_{c\,max}$ was not especially small. The results are in accordance with the relationship predicted by the weakest link model (K_{Jc} ($\propto J_c^{1/2}$) $\propto B^{(-1/4)}$) [11].

Note that, though the $J_{c\,max}$ shows TST dependence, it is interesting that K_{max} in Table 4 shows little dependence on TST.

2. 4. Finite element analysis

2.4.1. Elastic analysis

Elastic FEA for three test specimen geometries fundamentally shown in Fig. 3 was conducted using WARP3D [17]. Deviation from the figure was that the crack length a, was set at the nominal value of 12.5 mm (a/W = 0.5) for all cases. 1/4 of the structure was analyzed, taking symmetry into account (Fig. 6(a)). 20-nodes hexahedral meshes were used in general. For all cases, the crack tip was modeled by singular elements, whose size Δl was set at 0.001 of crack length a, and the radius of the “spider web” around the crack tip was set at 20 Δl (Fig. 6 (b)). Young’s modulus E of 206 GPa and Poisson’s ratio ν of 0.3 were used in all cases.

Considering the fact that the average SIF at fracture K_{max} was around 66 MPam$^{1/2}$, regardless of specimen thickness as given in Table 4, the load was set to a value so that this K_{max} could be obtained using equation (3) (in concrete, P_{max} = 12, 9.6 and 6 kN for B/W = 0.5, 0.4. and 0.25, respectively).

SIF was evaluated by applying the domain integral method to the FEA results. T_{11} was obtained by applying the domain integral and interaction integral method [13] to the FEA results. This method for calculating various T_{11} solutions has been used widely in the past [12, 18-20]. Finally, T_{33} was evaluated from Eq. (2).

Figure 7 shows the dependence of K, T_{11} and T_{33} taken at the specimen thickness center on B/W. We focused on these specimen thickness center values considering them as representing the characteristic intensity over the thickness. Details of the K, T_{11} and T_{33} distribution along the specimen thickness are summarized in the Discussion. According to Fig. 7, the Ks were not affected by B/W as expected, and were close to the nominal 2D SIF of 66 MPam$^{1/2}$. T_{11} showed visible dependence on B/W, though the variation was less than 10%. In summary, the in-plane parameters at the specimen thickness center showed small TST dependence, as expected.

On the other hand, T_{33} showed strong dependence on B/W. T_{33} was negative for all cases that were considered, and approached zero as B/W increased. Considering the fact that negative T-stress corresponded to the loss in crack tip constraint [5], it appears that T_{33} represented the well known tendency that large out-of-plane crack tip constraint is expected for thick test specimens. Another finding was that T_{11} and T_{33} showed different signs. This fact does not contradict with the fact that T_{11} and T_{33} are independent, as reported by Qu and Wang [12].

Based on this result, additional analyses for the case of B/W = 0.6, 0.8 and 1.0 were made, expecting that T_{33} saturated to a specific value for a large B/W, corresponding to the saturation of fracture toughness for thick test specimens. For all cases, the effective thickness at side groove $B_N = 0.8\ B$, crack length $a = 0.5\ W$ and load corresponding to 2D nominal SIF of 66 $MPam^{1/2}$ was applied, as in the analysis summarized in Fig. 7. Material constants were identical to those in the previous cases. The results are compiled in Fig. 8 (a) and (b). Results from Fig. 7 were also included.

According to Fig. 8 (a), $|T_{33}|$ decreased linearly with the increase in B/W, in the range of $0.25 \le B/W \le 0.5$ (0.5 is a standard value). Because W was kept constant for all the analyses, the following relationship was deduced.

$$\left|T_{33}\right| \propto B^{-1} \quad (\,for\; 0.25 \le B/W \le 0.5) \tag{4}$$

On the other hand, when B/W exceeded 0.5, the negative T_{33} seemed to show an upper bound value with the increase in B/W (Fig. 8 (b)). Assuming that increase in T_{33} represent the increase in crack tip constraint, the T_{33} tendencies with B/W seemed to be consistent with the well known relationship between fracture toughness and test specimen thickness. By combining the relationship obtained for 0.55% carbon steel S55C in Fig. 5, i.e., $J_{c\ max} \propto B^{-1/2}$ for $0.25 \le B/W \le 0.5$, the following expression is suggested as a possible relationship.

$$J_c \propto \left|T_{33}\right|^{1/2} \quad (\,for 0.25 \le B/W \le 0.5) \tag{5}$$

Note that the T_{33} results (Eq. (4)) were for loads corresponding to nominal 2D SIF of 66 MPam$^{1/2}$ for all cases, based on the experimental result that SIF at fracture was close to this value, as shown in Table 4. Thus, in order for equation (5) to be valid, the J obtained by elastic-plastic FEA for the maximum load corresponding to nominal 2D SIF of 66 MPam$^{1/2}$, hereafter called J_{FEA}, should show the relationship $J_{FEA} \propto B^{-1/2}$ for $0.25 \leq B/W \leq 0.5$. Thus in the following, we report elastic-plastic FEA results for cases of $B/W = 0.25$, 0.4 and 0.5.

2.4.2. Elastic-plastic analysis

FEA model used in the elastic-plastic analysis was basically the same as that used in the elastic analysis. The exception was the crack tip elements. In order to run large strain analysis, singular elements were removed so that a circular hole with radius of ρ = 0.0125 mm was inserted at the crack tip for all cases (Fig. 9).

Besides the E and ν, the Ramberg-Osgood approximation given in equation (6) was applied. Here, the parameters were set at α = 1.61, n = 6.90 and σ_0 = 428 MPa, determined as an average of the two tensile test data.

$$\frac{\varepsilon}{\varepsilon_0} = \frac{\sigma}{\sigma_0} + \alpha \left(\frac{\sigma}{\sigma_0} \right)^n \tag{6}$$

Maximum load was set as identical with the P_{max} used in the elastic analysis, corresponding to 2D nominal SIF of 66 MPam$^{1/2}$. In concrete, P_{max} was set at 12, 9.6 and 6 kN for B/W = 0.5, 0.4 and 0.25, respectively. J was extracted by applying the domain integral method to the FEA results. J, taken at the specimen center under P_{max}, designated as J_{FEA}, was added to Fig. 5 and presented as Fig. 10. WARP3D [17] was used for this elastic-plastic analysis.

Figure 10 confirms that J_{FEA}, which corresponds to the 2D nominal SIF of 66 MPam$^{1/2}$, is proportional to $(B/W)^{-1/2}$ for $0.25 \leq B/W \leq 0.5$, similar to the fracture toughness $J_{c\,max}$, as expected. Considering the fact that the relationship $J_{FEA} \propto B^{-1/2}$ and $|T_{33}| \propto B^{-1}$ (Eq.(4)) were obtained for the identical P_{max}, the proposed equation, Eq. (5), offers a correct description. We anticipate that other researchers that study this problem will validate Eq. (5) for other materials, which is also our future plan. In addition, we have a future plan to validate the relationship given in Eq. (5) for other types of fracture toughness test specimens.

2.5. Proposal of experimental formulation: TST effect on fracture toughness with T_{33} for S55C

From the discussion above, the TST effect observed for S55C tested by CT specimen was compiled in Fig. 11 and is formulated in terms of T_{33}, as follows.

$$J_c\,[\mathrm{N/mm}] = 3[\mathrm{N}^{1/2}]\cdot\left|T_{33}\right|^{1/2} \qquad (\mathit{for\ S55C\ at}\ 20^{\circ}\mathrm{C}; 60 \leq \left|T_{33}\right| \leq 200\,\mathrm{MPa}) \tag{7}$$

3. Discussions

In this work, the TST effect on fracture toughness observed for S55C, which is in the transition temperature range, was compiled in general form as Eq. (5) and material specific form as Eq. (7). In these empirical equations, the TST effect was described with a single out-of-plane elastic parameter T_{33} taken at the specimen thickness center. Though the depicted relationship between the fracture toughness of a material and T_{33} has to be validated for other materials and other type of test specimen configurations, using T_{33} as a relevant constraint parameter is definitely worth further investigation.

It could be argued that the relationship $J_c \propto (B^{(-1/2)}) \propto |T_{33}|^{1/2}$ (Eq (5)) is in accordance with, but no more than what is predicted by the weakest link model (K_{Jc} ($\propto J_c^{1/2}$) $\propto B^{(-1/4)}$)) [11]. However, as Anderson et al. pointed out, as a contradiction of the weakest link model, "fracture toughness does not decrease indefinitely with thickness [11]." On the other hand, $|T_{33}|$ seemed to saturate to a lower bound for $B/W > 1$ (Fig. 8 (a) and (b)). On the point that $|T_{33}|$ seemed to show a lower bound for large B/W, it seems that T_{33} has the potential to predict what B/W is enough to obtain a lower bound fracture toughness and conquer the limitation of the weakest link model. Further study on this is also in our future plan.

Rigorously speaking, Eq. (7) is valid for S55C tested with CT specimens of W = 25 mm at 20 ^{O}C. However, the more general relationship given in Eq. (5) should be valid to express the TST effect tested under a various combinations of material, W and test temperature. Thus, the primary use of Eq. (5) is expected to be in situations such as converting the fracture toughness J_c obtained from a non-standard B/W specimen to that for B/W = 0.5 (standard specimen). Another expected future application of Eq. (5) is in predicting a fracture toughness of a surface crack in a structure from J_c obtained using a CT specimen, assuming that test specimen could be prepared so that the (K, T_{11}) combination (or ratio) in both the structures is identical (for example, by adjusting test specimen's T_{11} with a/W), and considering the difference in T_{33} by Eq. (5). Our next effort will be to validate Eq. (5) for different materials and test specimens *W*s.

In Fig. 7, the TST effect in *K*, T_{11} and T_{33} is shown at the specimen thickness center. It is true that these values distribute in the specimen thickness direction, as shown in Fig. 12 (Note that 80% of (B_N/2) was considered for x_3, because *T* stresses at or in the vicinity of the free surfaces are known to be unreliable [12]). There are many possibilities to treat this 3D effect, but considering the fact that the fracture tends to initiate at the specimen thickness center, the values at specimen thickness center were chosen to represent the characteristic intensity of these values.

4. Conclusions

In this work we focused on the elastic parameter T_{33} (the out-of-plane non-singular term in the series of elastic crack-tip stress fields), expecting that T_{33}-stress affected the crack-tip triaxiality and thus constraint in the out-of-plane direction. Fracture toughness tests with CT test specimens, which had the same in-plane geometry and different thickness, were conducted to determine the TST (Test Specimen Thickness) effect on fracture toughness. In additions to these tests, 3D elastic FEA was conducted for the different test specimens under identical nominal 2D SIF. This load was selected because fracture toughness in terms of SIF had little TST dependence. The 3D elastic FEA results showed small TST dependence for the in-plane elastic parameters *K* and T_{11}, and large dependence for the out-of-plane parameter T_{33}. Another finding was that T_{33}, which was negative, seemed to show an upper bound for large specimen thickness. Next, elastic-plastic FEA corresponding to the test results were run for comparison. The results reproduced the TST effect on fracture toughness test in terms of J ($J_c \propto B^{-1/2}$), and finally this TST effect was formulated as $J_c \propto |T_{33}|^{1/2}$ for $0.25 \leq B/W \leq 0.5$. In addition to the fact that $|T_{33}|$ seemed to show a lower bound for large B/W, these results seem to indicate the possibility of improving the existing methods for correlating fracture toughness obtained in test specimens with the toughness of actual cracks found in the structure, using T_{33}.

Acknowledgement

Part of this work was supported by Japan Nuclear Energy Safety Organization. Their support is greatly appreciated.

References

[1] Shih, C. F. and German, M. D. Requirements for a One Parameter Characterization of Crack Tip Fields by the Hrr Singularity. International Journal of Fracture. 1981;**17**(1):27-43.

[2] Larsson, S. G. and Carlsson, A. J. Influence of Non-Singular Stress Terms and Specimen Geometry on Small-Scale Yielding at Crack Tips in Elastic-Plastic Materials. Journal of the Mechanics and Physics of Solids. 1973;**21**(4):263-277.

[3] Williams, M. L. On the Stress Distribution at the Base of a Stationary Crack. Journal of applied mechanics. 1957;**24**:111-114.

[4] Rice, J. R. Limitations to the Small Scale Yielding Approximation for Crack Tip Plasticity. Journal of the Mechanics and Physics of Solids. 1974;**22**(1):17-26.

[5] Bilby, B. A., Cardew, G. E., Goldthorpe, M. R. and Howard, I. C. A Finite Element Investigation of the Effect of Specimen Geometry on the Fields of Stress and Strain at the Tips of Stationary Cracks. . Size Effects in Fracture. London: Mechanical Engineering Publications Limited, 1986. p. 37-46.

[6] Al-Ani, A. M. and Hancock, J. W. J-Dominance of Short Cracks in Tension and Bending. Journal of the Mechanics and Physics of Solids. 1991;**39**(1):23-43.

[7] Betegon, C. and Hancock, J. W. Two-Parameter Characterization of Elastic-Plastic Crack-Tip Fields. Journal of applied mechanics. 1991;**58**(1):104-110

[8] Du, Z. Z. and Hancock, J. W. The Effect of Non-Singular Stresses on Crack-Tip Constraint. Journal of the Mechanics and Physics of Solids. 1991;**39**(4):555-567.

[9] O'dowd, N. P. and Shih, C. F. Family of Crack-Tip Fields Characterized by a Triaxiality Parameter--I. Structure of Fields. Journal of the Mechanics and Physics of Solids. 1991;**39**(8):989-1015.

[10] Kirk, M. T., Dodds, R. H. and Anderson, T. L. An Approximate Technique for Predicting Size Effects on Cleavage Fracture Toughness (J_c) Using the Elastic *T* Stress In: Landes, J. D., Mccabe, D. E. and Boulet, J. a. M., editors. Stp 1207, Fracture Mechanics: Twenty-Fourth Volume Philadelphia: American Society for Testing and Materials, 1994. p. 62-86.

[11] Anderson Ted, L., Stienstra, D. and Dodds Robert, H. A Theoretical Framework for Addressing Fracture in the Ductile-Brittle Transition Region. In: Landes John, D., Mccabe Donald, E. and M., B. J. A., editors. Fracture Mechanics: 24th Volume. Philadelphia: American Society for Testing and Materials, 1994. p. 186-214.

[12] Qu, J. and Wang, X. Solutions of T-Stresses for Quarter-Elliptical Corner Cracks in Finite Thickness Plates Subject to Tension and Bending. International Journal of Pressure Vessels and Piping. 2006;**83**(8):593-606.

[13] Nakamura, T. and Parks, D. M. Determinationof Elastic T-Stress Along Three-Dimensional

Crack Fronts Using an Interaction Integral. International journal of solids and structures. 1992;**29**(13):1597-1611.

[14] Jis. Z2241 Method of Tensile Test for Metallic Materials. Tokyo: Japanese Industrial Standards Committee, 1998.

[15] Astm, E. E399-05 Standard Test Method for Plane-Strain Fracture Toughness of Metallic Materials. Annual Book of Astm Standards. Philadelphia PA: American Society for Testing and Materials, 2005.

[16] Astm, E. E1820-06a Standard Test Method for Measurement of Fracture Toughness. Annual Book of Astm Standards. Philadelphia PA: American Society for Testing and Materials, 2006.

[17] Gullerud, A., Koppenhoefer, K., Roy, Y., Roychowdhury, S., Walters, M., Bichon, B., Cochran, K. and Dodds Jr, R. Warp3d Release 15 Manual. Civil Engineering, Report No UIUCENG-95-2012, University of Illinois at Urbana-Champaign. 2004.

[18] Wang, X. and Bell, R. Elastic T-Stress Solutions for Semi-Elliptical Surface Cracks in Finite Thickness Plates Subject to Non-Uniform Stress Distributions. Engineering Fracture Mechanics. 2004;**71**(9-10):1477-1496.

[19] Zhao, J., Guo, W. and She, C. The in-Plane and out-of-Plane Stress Constraint Factors and K - T - Tz Description of Stress Field near the Border of a Semi-Elliptical Surface Crack. International Journal of Fatigue. 2007;**29**(3):435-443.

[20] Lewis, T. and Wang, X. The T-Stress Solutions for through-Wall Circumferential Cracks in Cylinders Subjected to General Loading Conditions. Engineering Fracture Mechanics. 2008;**75**(10):3206-3225.

List of Tables

Table 1 Chemical composition of test specimens

C	Si	Mn	P	S	Cu	Ni	Cr	Nb	B	Fe
0.54	0.18	0.64	0.018	0.002	0.01	0.01	0.01	-	-	Bal.

Table 2 Mechanical properties of test specimens

Yield Stress σ_{YS} MPa	Tensile Strength σ_B MPa	Young's Modulus E GPa	Elongation %
470, 386	701, 680	206*	25.8, 27.2

*: Reference value

Table 3 Details of fatigue precracking procedure

B/W	Serial No.	1	2	3	4	5
0.25	P_{max} N	1 830				
	P_{min} N	183				
	K_{max} MPam$^{1/2}$	19.5	19.6	19.6	19.6	19.2
	Number of cycles	350 920	307 810	319 630	278 960	354 290
0.4	P_{max} N	2 930				
	P_{min} N	293				
	K_{max} MPam$^{1/2}$	19.2	19.2	18.9	19.2	19.5
	Number of cycles	298 450	290 270	271 380	295 660	386 220
0.5	P_{max} N	3 660				
	P_{min} N	366				
	K_{max} MPam$^{1/2}$	18.9	18.9	19.0	19.9	19.3
	Number of cycles	328 480	260 850	255 810	319 500	373 020

Table 4 Results of fracture toughness tests

B/*W*	Serial No.	1	2	3	4	5
0.25	*a*/*W*	0.49	0.49	0.49	0.49	0.49
	P_{max} kN	6.67	5.72	5.32	5.79	6.92
	K_{max} MPam$^{1/2}$	71.03	61.17	56.82	61.90	72.49
	$J_{c\ max}$ N/mm	94.35	22.76	18.72	24.10	42.84
	Loading Rate MPam$^{1/2}$/sec	0.74	1.12	1.08	1.10	1.02
0.4	*a*/*W*	0.49	0.49	0.48	0.49	0.49
	P_{max} kN	9.71	10.29	7.50	6.73	9.64
	K_{max} MPam$^{1/2}$	63.65	67.67	48.48	43.99	63.98
	$J_{c\ max}$ N/mm	24.44	30.70	12.64	10.21	24.56
	Loading Rate MPam$^{1/2}$/sec	1.25	1.32	1.26	1.26	1.33
0.5	*a*/*W*	0.48	0.48	0.48	0.50	0.49
	P_{max} kN	13.65	13.33	8.77	11.10	12.14
	K_{max} MPam$^{1/2}$	70.88	68.52	45.54	60.25	63.77
	$J_{c\ max}$ N/mm	31.46	30.42	10.94	21.04	24.72
	Loading Rate MPam$^{1/2}$/sec	1.20	1.26	1.09	1.21	1.15

List of Figures

Figure(s)

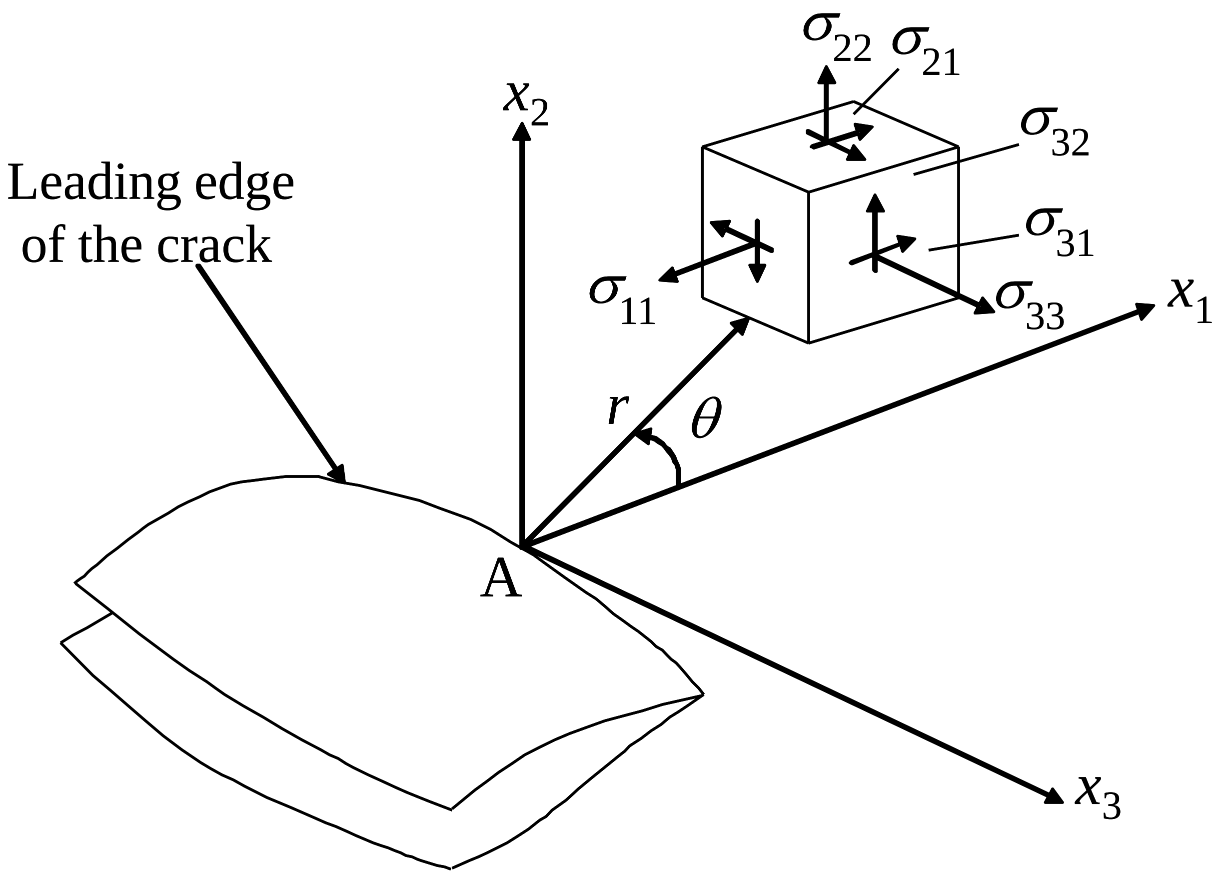

Fig. 1 Three-dimensional coordinate system for the region along the crack front

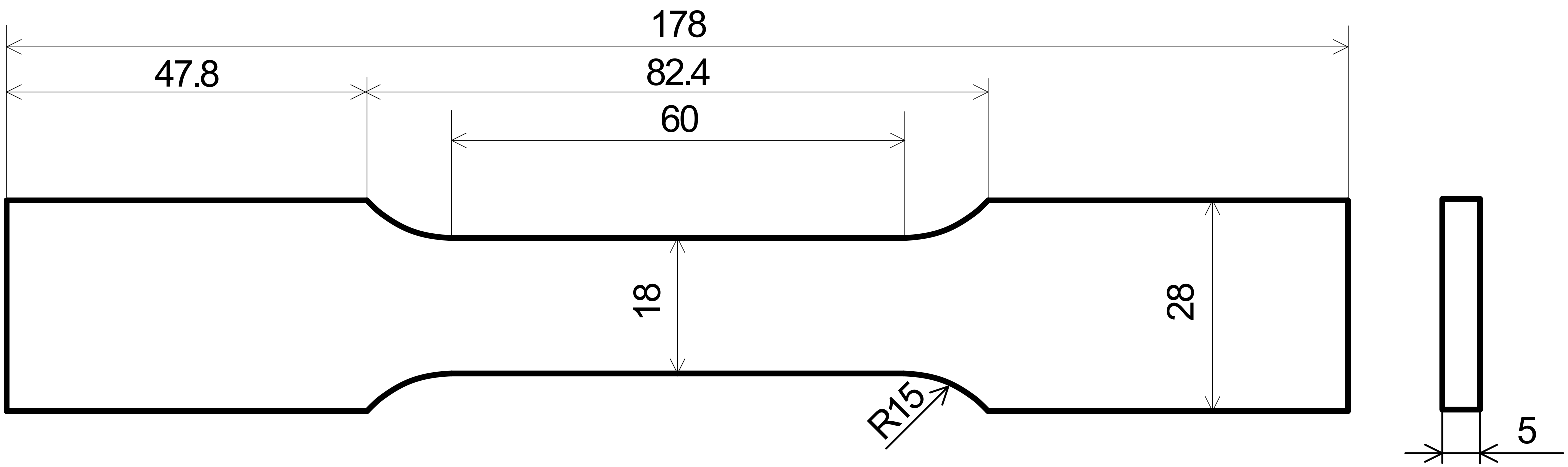

Fig. 2 Tensile specimen configuration

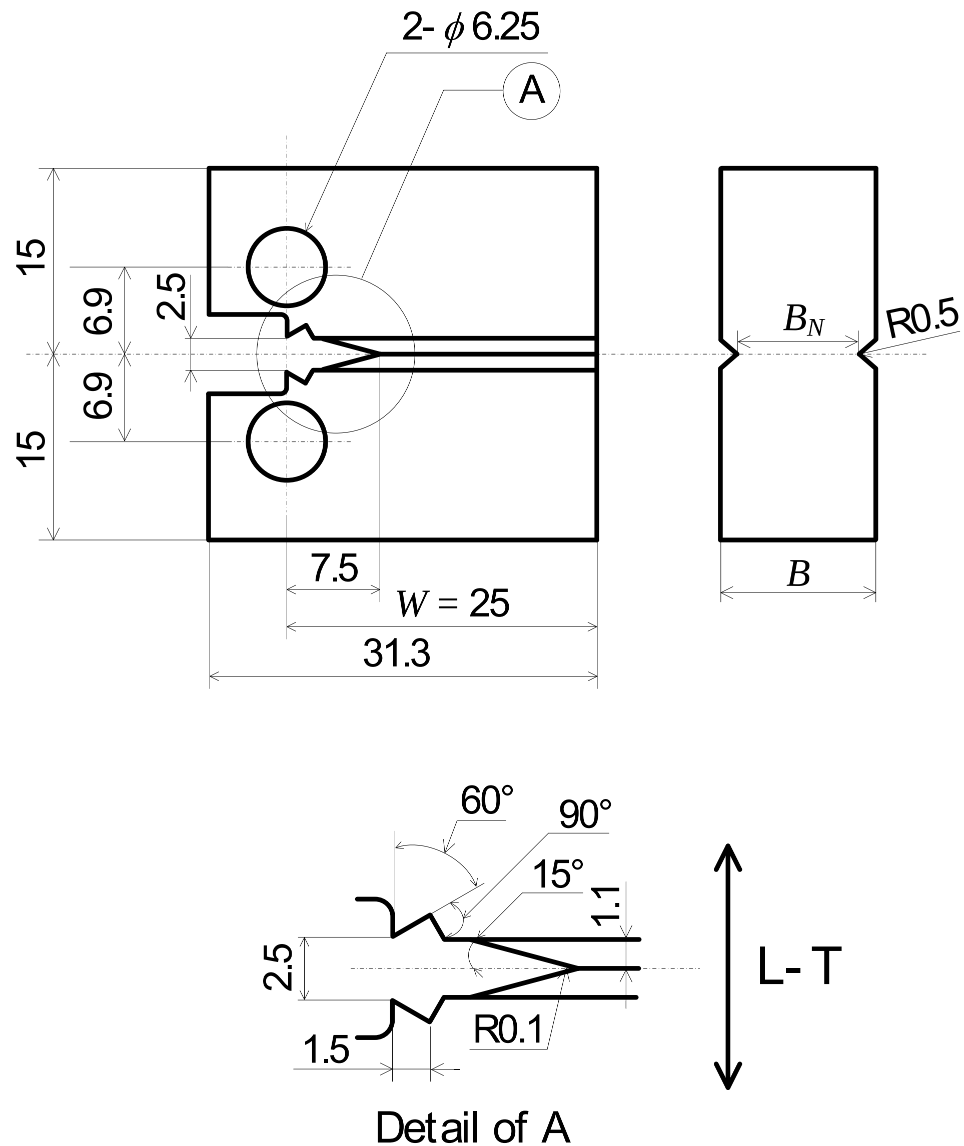

Fig. 3 CT specimen configuration

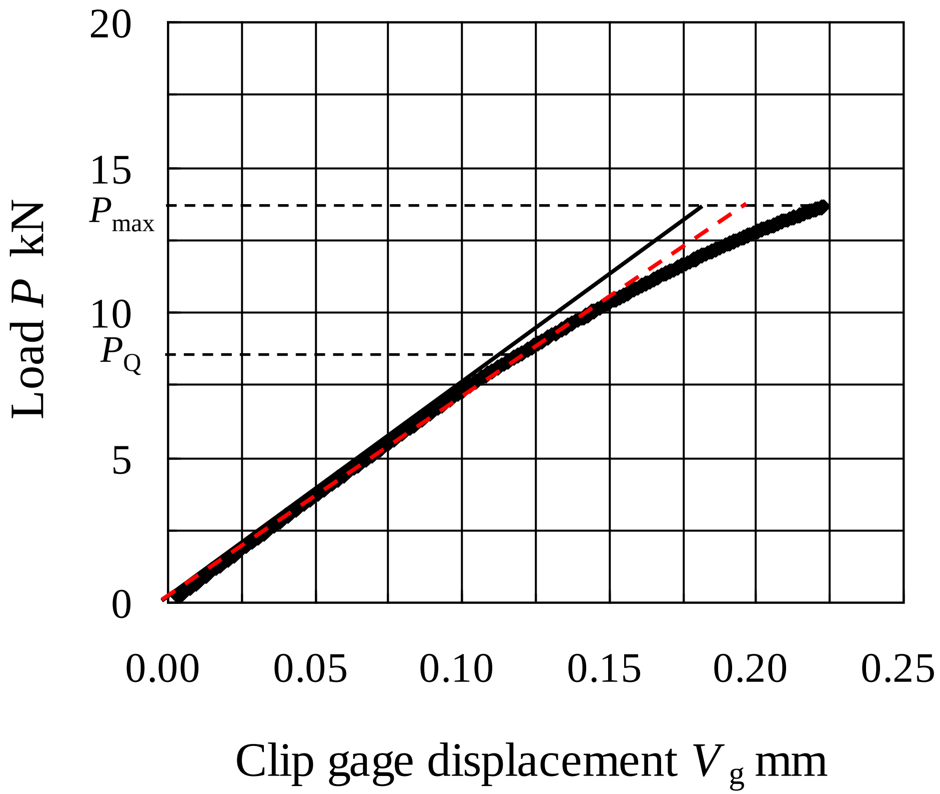

Fig. 4 Typical load-displacement (P-V) curve for CT specimen (*B*/*W* = 0.5, test piece no.1)

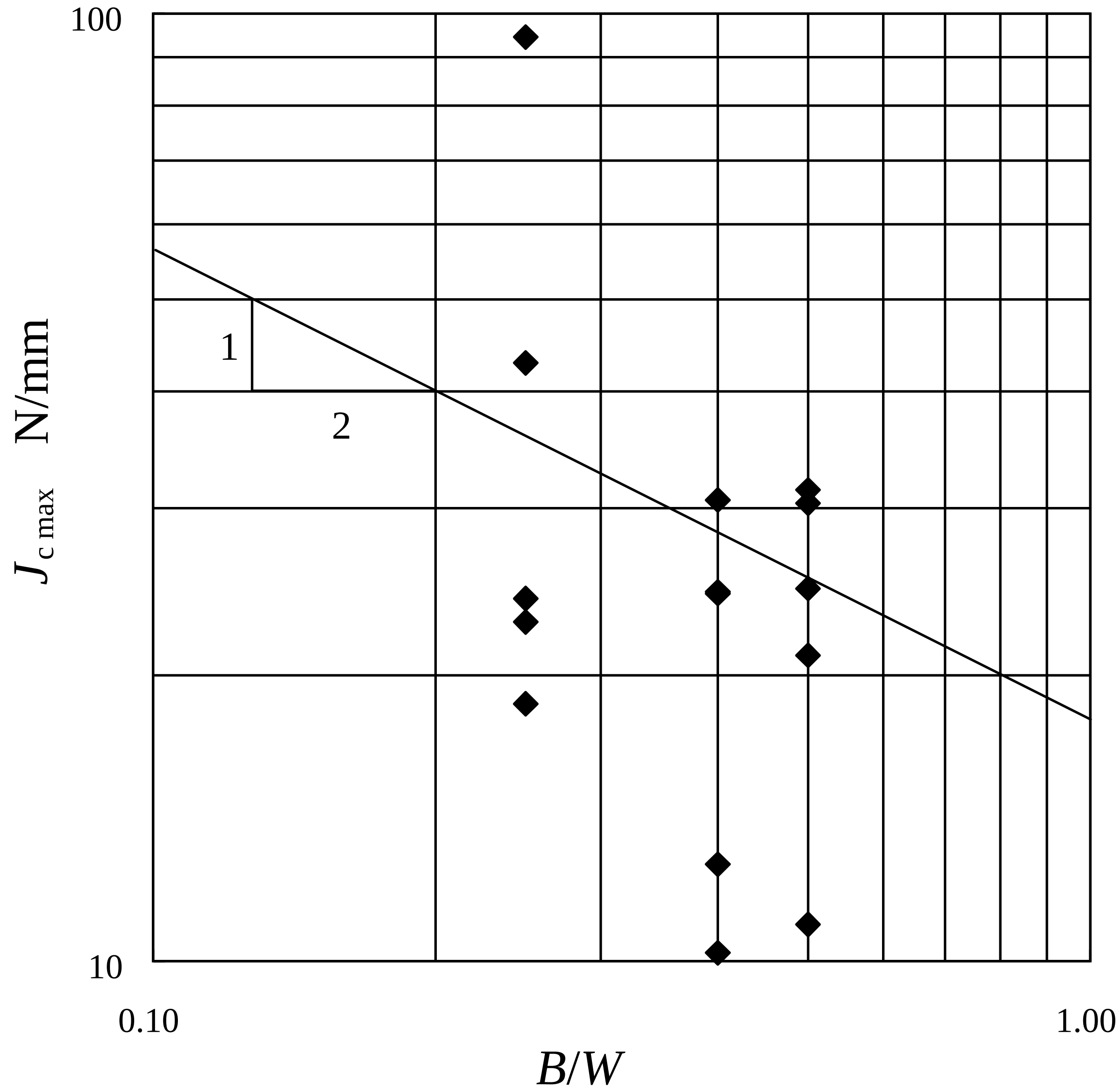

Fig. 5 Relationship between $J_{c\,max}$ and B/W (S55C)

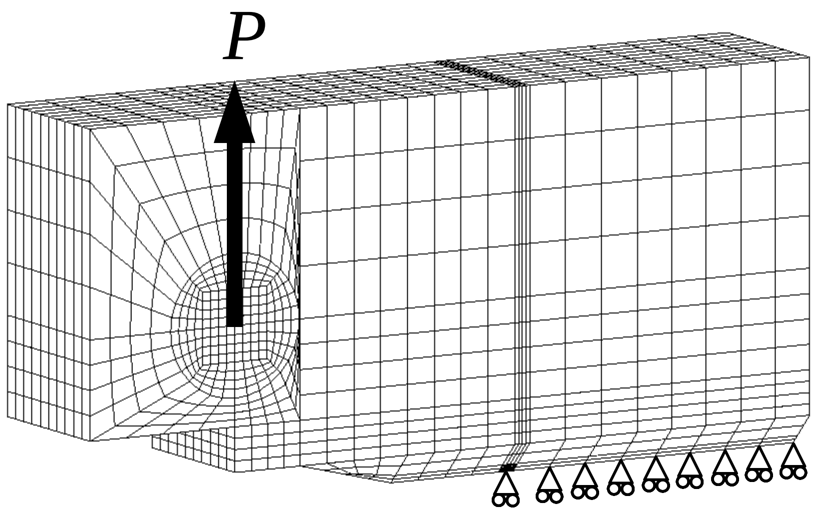

(a) Global mesh

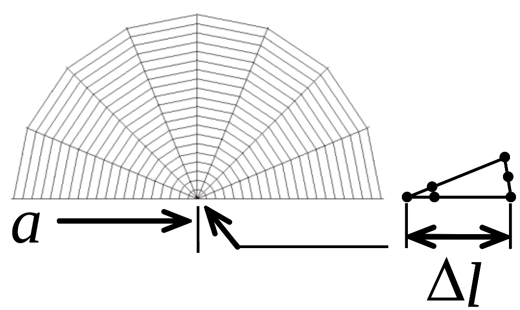

(b) Detail of crack tip for elastic analysis

Fig. 6 Finite element model of CT specimen

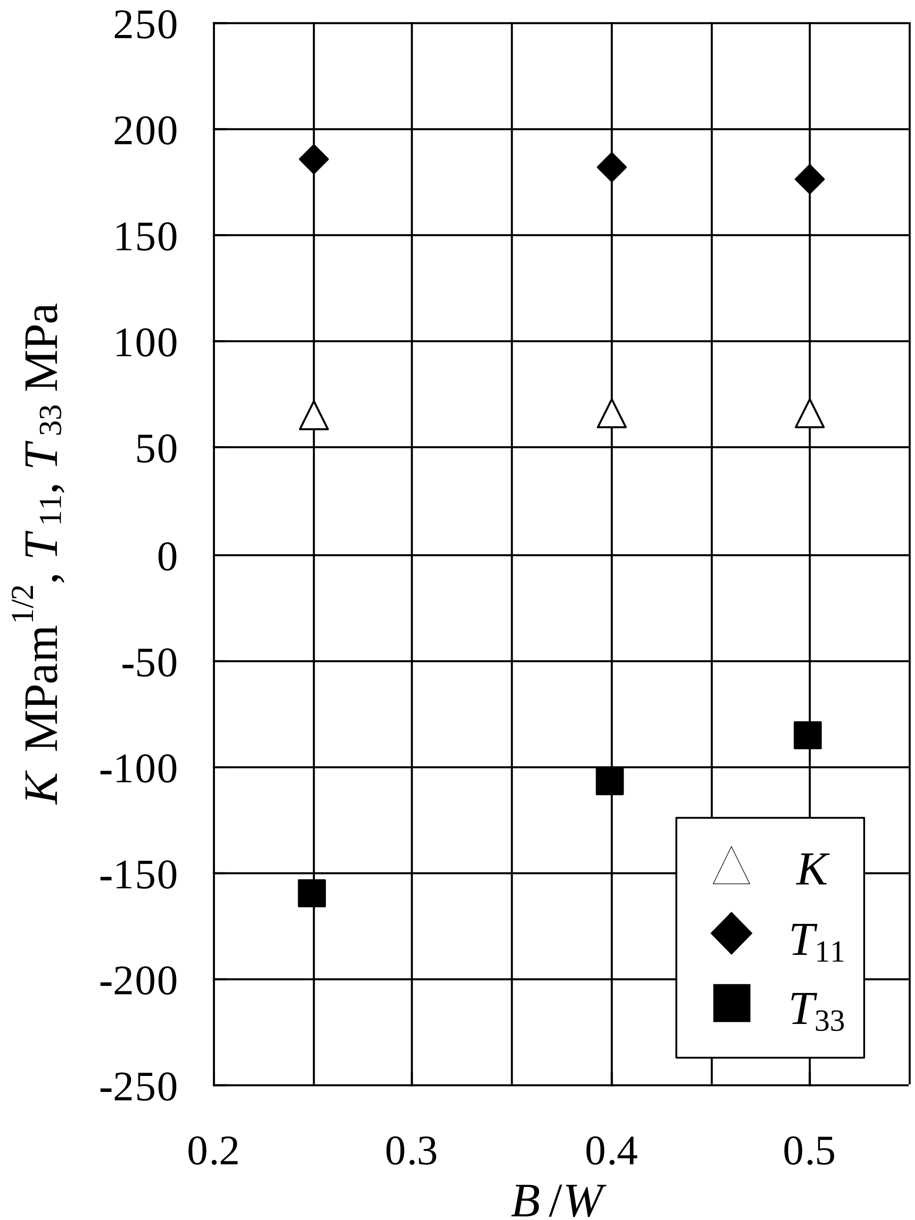

Fig. 7 Comparison of K, T_{11} and T_{33} at CT specimen thickness center for a load corresponding to nominal SIF of 66 $MPam^{1/2}$ ($\nu = 0.3$)

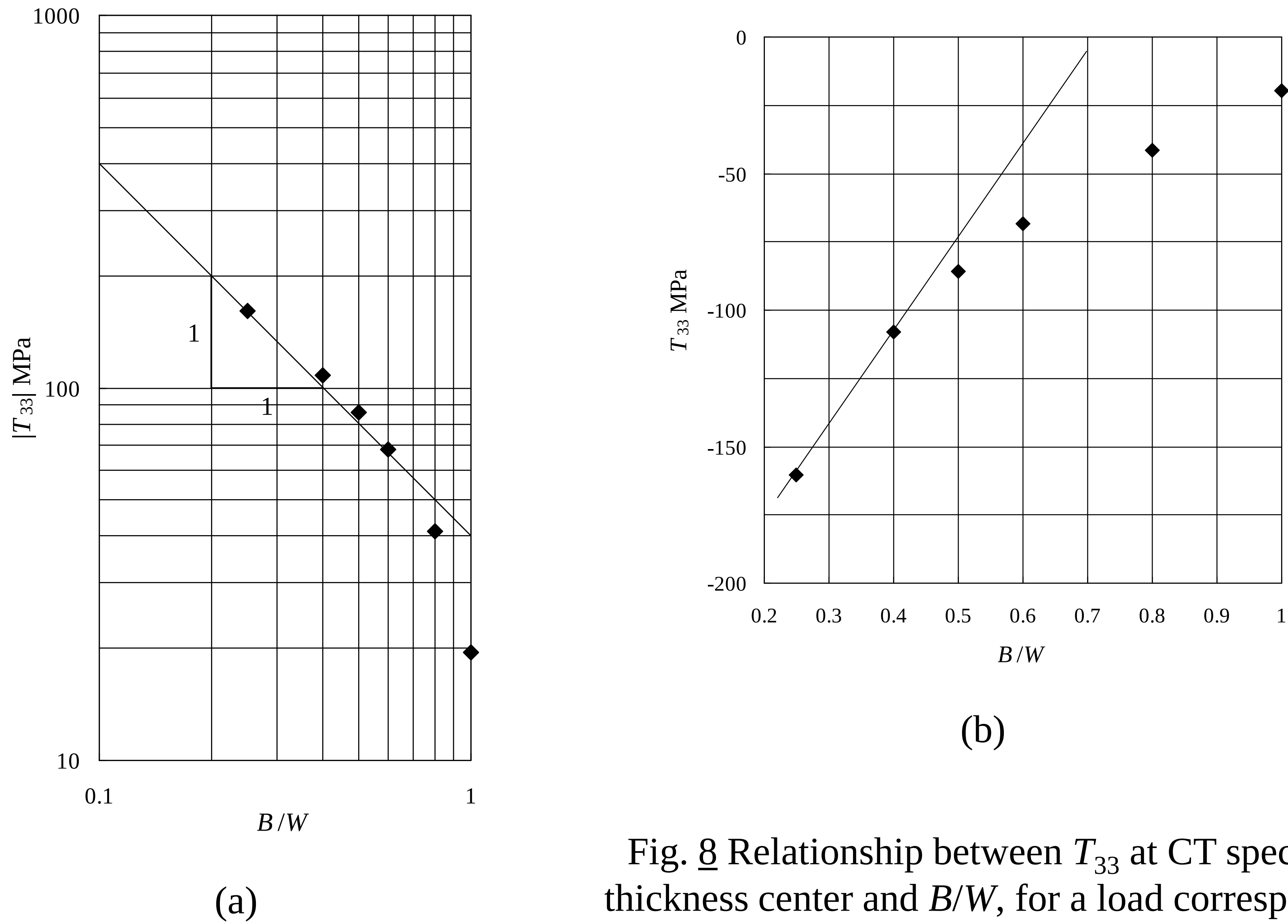

Fig. 8 Relationship between T_{33} at CT specimen thickness center and B/W, for a load corresponding to nominal SIF of 66 MPa$^{1/2}$ ($\nu = 0.3$)

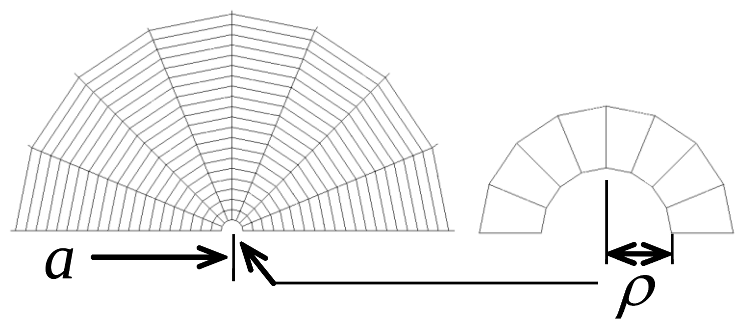

Fig. 9 Finite element model for elastic-plastic analysis at the crack tip

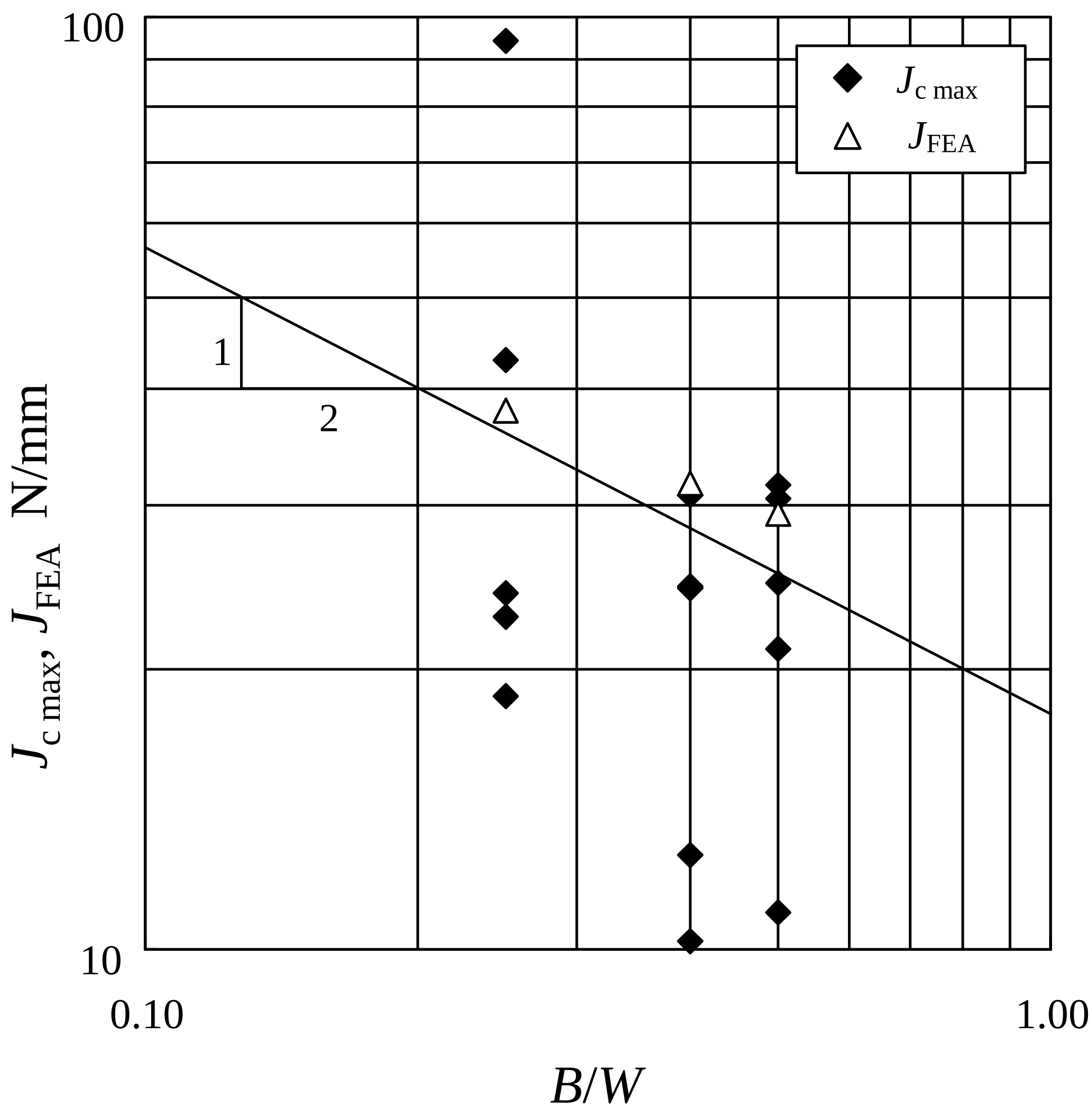

Fig. 10 Relationship between $J_{c\,max}$, J_{FEA} and B/W (S55C)

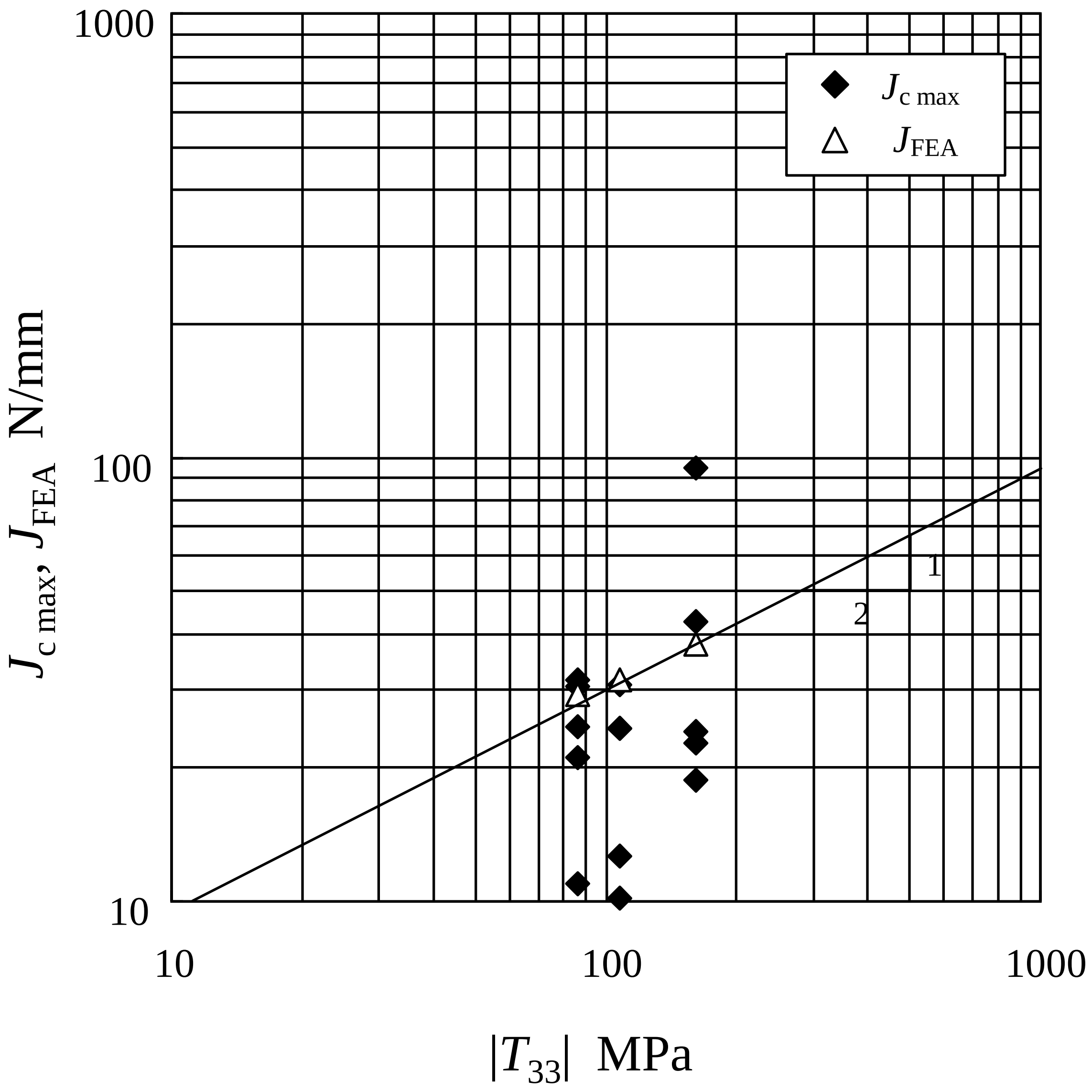

Fig. 11 Relationship between $J_{c\,max}$, J_{FEA} and $|T_{33}|$ (S55C)

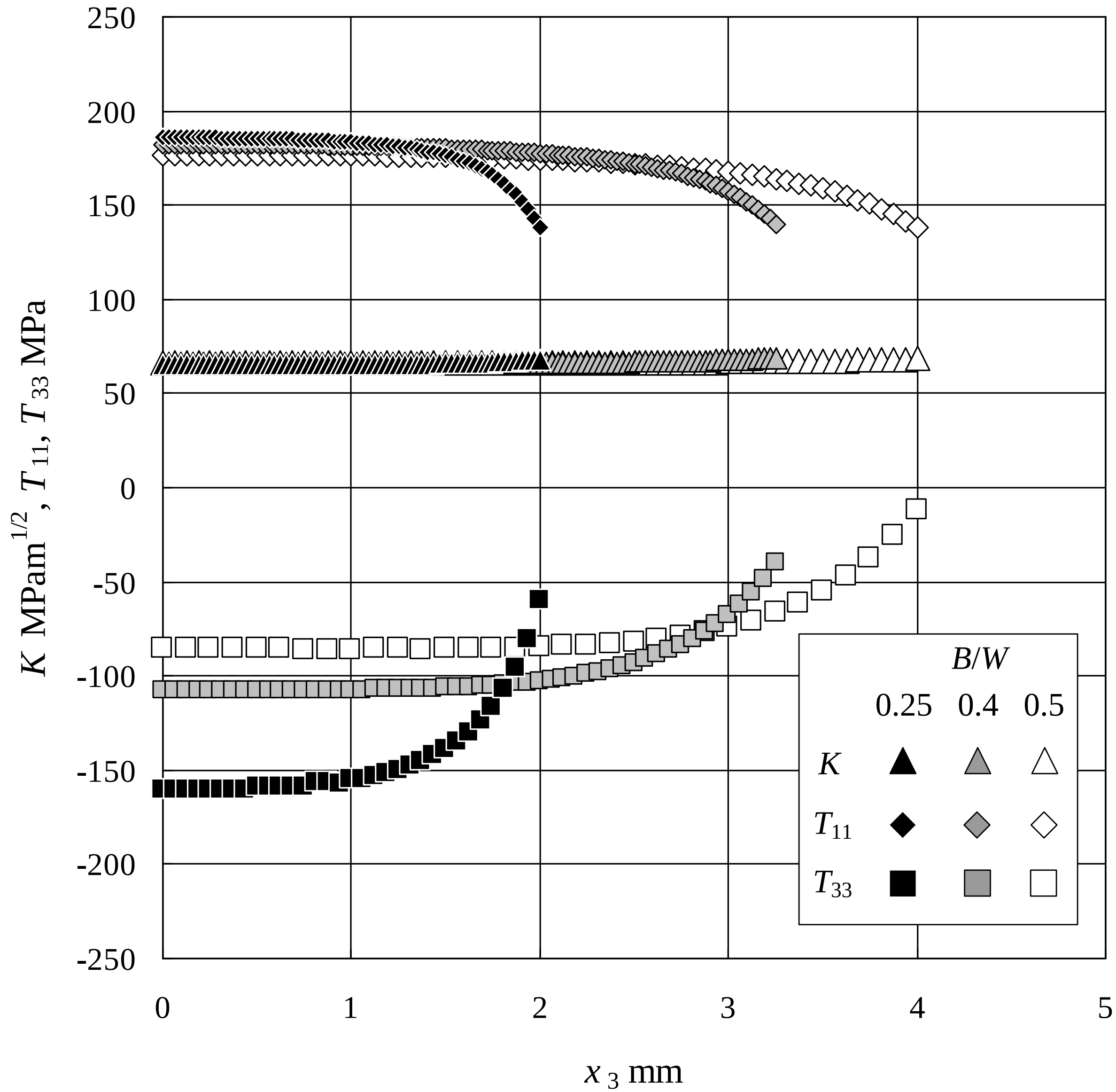

Fig. 12 Variation of K, T_{11} and T_{33} along the crack front for a load corresponding to nominal SIF of 66 MPa$^{1/2}$ ($\nu = 0.3$)